Power losses comparison between Silicon Carbide and Silicon devices for an isolated DC-DC converter

Filippo Pellitteri, Alessandro Busacca, Carmelo Martorana, Rosario Miceli, *IEEE member*, Salvatore Stivala
Department of Engineering
University of Palermo
Palermo, Italy
filippo.pellitteri@unipa.it

Angelo Alberto Messina
STMicroelectronics ; IMM, CNR
Catania, Italy
angelo.messina@st.com

Michele Calabretta, Vincenzo Vinciguerra
ADG R&D
STMicroelectronics
Catania, Italy
michele.calabretta@st.com

***Abstract*—In recent years, new efficient power devices have been implemented; in particular, Silicon Carbide (SiC) devices have advantages as regards their electrical characteristics, such as very low power losses, low gate charge, low capacitances, a low on-state resistance and many others, when compared to the Silicon (Si) devices; these devices can operate at high switching frequency and high voltages; with reference to their thermal characteristics, thanks to their great thermal conductivity, high power can be obtained and, because of their wide bandgap, high temperature can be reached; for these reasons, these devices are utilized in a wide range of technological applications, including power electronics. In this paper, power losses in Si and SiC devices are evaluated in simulation and compared to each other; in order to demonstrate the remarkable advantages of the SiC devices over the silicon ones, a study which makes use of an isolated DC-DC converter is proposed in this paper. As regards the proposed full-bridge converter, SiC and silicon MOSFETs and diodes, of whom some static and dynamic parameters are compared, are used in order to transfer power from a DC voltage supply to a load.**

Keywords—*SiC devices; isolated power converters; power losses; DC-DC converters.*

I. INTRODUCTION

With the development of new efficient power devices, new materials are used for replacing the traditional silicon power devices. In particular, Silicon Carbide (SiC) power devices may be defined as the future of electronics and the future of electronics and semiconductor industries, in so far as high switching frequency, low power losses and high voltages are the main features of these devices [1-2]. Because of their great thermal conductivity and wide bandgap, these ones can be exploited to get high power and to operate at high temperatures. These are the reasons why SiC plays an important role in the implementation of new technology applications, such as high efficiency DC-DC converters, DC-AC converters, inverters for solar and wind energy, photo-voltaic converters, power converters for electrical and vehicles, motor drives, power inverters for industrial equipment, high voltage switches for X-ray generators, thin-film coating processes, chargers and power supplies for renewable energy systems [3-16]. Many power devices are produced, such as Schottky barrier diodes, MOSFETs, power modules, IGBTs, BJTs, and many companies are engaged in making them. With reference to the electrical and thermal characteristics, SiC devices present advantages over the silicon ones. They offer a very high operating junction temperature capability, a low on-state resistance and an extremely low gate charge and input capacitance [17], offering the opportunity of efficient power converters with limited size, being energy saving and new electric storage solutions challenging topics for researchers [18-20].

The study proposed in this paper is part of the effort to demonstrate the remarkable advantages of SiC devices over the silicon ones. It makes use of the well-known full-bridge DC-DC converter [21]. In this paper, power losses in SiC devices are analyzed and compared to the silicon ones.

II. THEORETICAL OUTLINES

A. Conduction power losses and drain-source channel resistance

In order to minimize power losses, the transistors work as switches, either on or off, rather than working in their linear region [22]; nevertheless, the conduction power losses and the switching power losses must be taken into account: with reference to the first ones, when a transistor is on, the conduction losses are functional to the current and the channel resistance of the MOSFET. The conduction energy losses are calculated as follows [23]:

$$E_{cond}=\int_0^{D\cdot T_{sw}} i_d^2(t)\cdot R_{ds(ON)}dt \qquad (1)$$

where i_d is the drain current, D is the duty-cycle of the gate signal used to control MOSFET's logical state, T_{sw} is the switching period and $R_{ds(ON)}$ is the on-state drain-source channel resistance.

Conduction losses can be obtained in this way [23-24]:

$$P_{cond}=E_{cond}\cdot f_{sw}=D\cdot I_d^2\cdot R_{ds(ON)}=I_{d_{rms}}^2\cdot R_{ds(ON)} \qquad (2)$$

f_{sw} is the switching frequency and I_{drms} is the RMS value of the drain current. As can be seen, these losses depend on the duty-cycle.

Besides, the on-state drain-source channel resistance is functional to the junction temperature T_j [25]:

$$R_{ds(ON)}=R_{ds(ON)_t}\cdot[1+K\cdot(T_j-25°C)] \qquad (3)$$

where $R_{ds(ON)t}$ is the $R_{ds(ON)}$ calculated at 25°C, K is the thermal coefficient, obtained by the *normalized on-resistance vs. temperature* graphs from the datasheets.

This resistance is the sum of several resistive components originated from the technological steps that have led to the implementation of the MOSFET. These components are: the source region resistance, the channel resistance, the accumulation layer resistance, the drift region resistance and the drain region resistance. These ones are shown in Fig. 1.

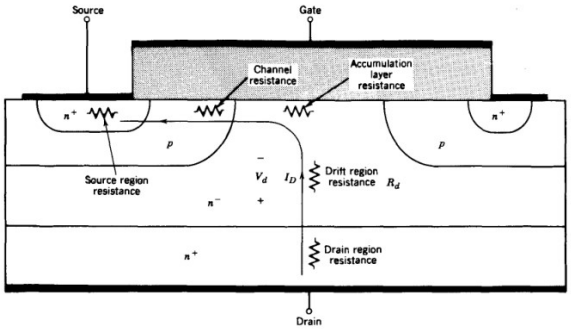

Fig. 1. Resistive components between source and drain [22]

In order to reduce all these contributions, the manufacturer uses the heaviest doping in each region. Furthermore, the extension of the gate metallization over the drift region is advantageous in terms of conductivity at the region between the drift region itself and the gate oxide, in so far as an accumulation layer is created [22].

With regard to the diodes conduction losses P_{cond_d} can be obtained in the same way [26]:

$$P_{cond_d}=f_{sw}\cdot\int_0^{T_{sw}} v(t)\cdot i(t)dt \quad (4)$$

where v(t) and i(t) are respectively the diode voltage and current, and T_{sw} is the switching period.

B. Switching power losses

With regard to the MOSFET switching power losses, these ones increase with the frequency. The turn-on losses are determined as follows [23]:

$$P_{turn_{on}}=E_{on}\cdot f_{sw} \quad (5)$$

E_{on} is the turn-on energy losses. This last one can be obtained as:

$$E_{on}=\int_0^{t_{d(on)}+t_r} v_{ds}(t)\cdot i_d(t)dt \quad (6)$$

$t_{d(on)}$ is the instant of time in which the on-transition starts, t_r is the current rise-time, v_{ds} and i_d are the drain-source and drain current during this interval time.

In the same way, turn-off losses can be calculated:

$$P_{turn_{off}}=E_{off}\cdot f_{sw} \quad (7)$$

E_{off} is the turn-off energy losses. It can be obtained by:

$$E_{off}=\int_0^{t_{d(off)}+t_f} v_{ds}(t)\cdot i_d(t)dt \quad (8)$$

$t_{d(off)}$ is the instant of time in which the off-transition starts and t_f is the current fall-time.

Switching losses are the sum of turn-on and turn-off power losses, so that:

$$P_{sw}=(E_{on}+E_{off})\cdot f_{sw} \quad (9)$$

Moreover, it's worth remembering that one of the most responsible elements of a MOSFET producing switching power losses is its body-diode, which is traversed by current during the t_{rr} reverse recovery time. This interval time is defined in Fig. 2 [27].

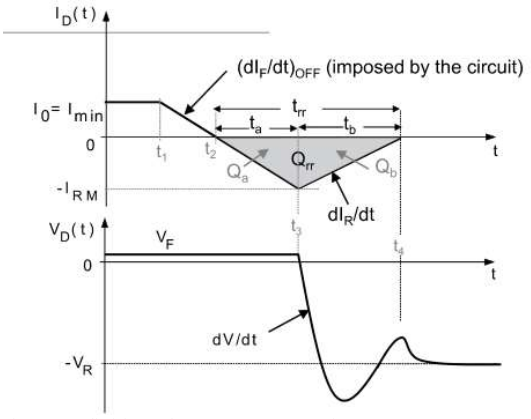

Fig. 2. Definition of reverse recovery time [28]

Q_{rr} is the stored charge; in fact, both for diodes and MOSFET body-diodes, this charge, called reversed recovery charge, can be calculated [28]:

$$Q_{rr}=\int_{t_2}^{t_2+t_a+t_b} I_d(t)dt \quad (10)$$

where $I_d(t)$ is the current.

With reference to Fig. 2, turn-off power losses are [28]:

$$P_{turn_{off}}=f_{sw}\cdot\int_{t_1}^{t_4} V_d(t)\cdot I_d(t)dt \quad (11)$$

where $V_d(t)$ is the diode reverse voltage.

It is also possible to obtain this charge by integrating the datasheet curves *typical capacitance vs. reverse voltage* V_R [29].

The switching performance related to a MOSFET is discussed in [2].

III. Analysis of the Isolated Converter

The well-known topology of the full-bridge converter is shown in Fig. 3: a DC voltage supplies the full-bridge inverter on the primary side of the transformer, made of n-channel MOSFETs T_1-T_2-T_3-T_4; the high-frequency transformer guarantees electrical isolation; a conventional four-diode rectifier on the secondary side of the transformer powers the DC load.

The DC-DC converter behaviour has been investigated via simulation, comparing the results among two cases: use of SiC devices and use of Si devices. The circuit uses both SiC and Si power devices in order to transfer power from the supply voltage to the output load.

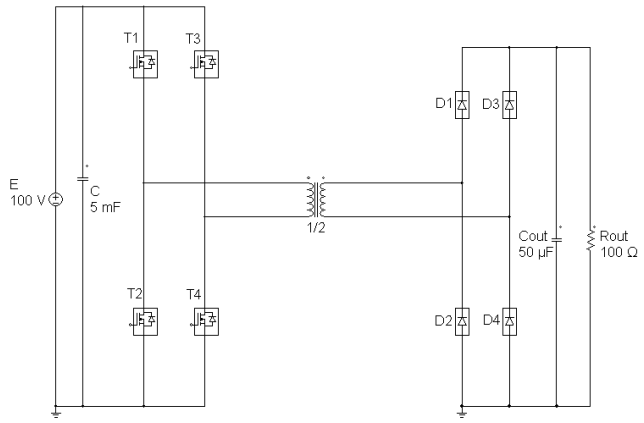

Fig. 3. Topology of the full-bridge converter

All the switching semiconductor devices have been accurately modeled in order to perform *PowerSIM* simulations.

Since the supply voltage may fluctuate, in order to provide to the MOSFETs a voltage as stable as possible, an electrolytic capacitor is used.

The transformer parameters are summarized in Table I.

TABLE I. TRANSFORMER PARAMETERS

Parameter	Value
Primary winding resistance	10 mΩ
Secondary winding resistance	10 mΩ
Leakage primary inductance	1µH
Leakage secondary inductance	1µH
Magnetizing inductance	100µH
Turns-ratio	1/2

A. Devices utilized

Regarding the full-bridge inverter MOSFETs, the SiC and the Si models used in simulation are those of the devices *SCTH40N120G2V7AG* and *IRFB4410ZPbf* respectively. Table II shows the main features of these devices [17, 30].

TABLE II. SIC AND SI MOSFETS FEATURES

Parameter	SiC	Si
C_{iss}	1230 pF	4820 pF
C_{oss}	56 pF	340 pF
C_{rss}	15 pF	170 pF
$R_{ds\text{-}on}$	75 mΩ	9 mΩ
Maximum I_d (at 25 °C)	33 A	97 A
Maximum V_{ds}	1200 V	100 V
t_{rr} (at 25°C)	10 ns	57 ns

In the full-bridge diode rectifier, the simulated models of SiC and Si are those of the devices *IDD05SG60C* and *MUR3020WT* respectively. Some features of these diodes are shown in Table III [31-32].

TABLE III. SIC AND SI DIODES FEATURES

Parameter	SiC	Si
Maximum continuous forward current	5 A	15 A
DC blocking voltage	600 V	200 V
t_{rr}	0	35 ns
Q_{rr}	0	19 nC

B. Power modulation

In order to compare SiC and Si performances, an efficiency investigation has been carried out on the proposed converter. Even though all simulations have been performed in open-loop configuration, a fixed target load power level has been chosen, equal to 200 W.

To modulate the load power, the active full-bridge on the primary side shall be properly controlled: a pulse width modulation (PWM) control on the MOSFETs logical state has been selected.

In order to control the logical state of each primary full-bridige MOSFET, phase-shifted PWM gate signals are used.

With reference to the full-bridge converter topology, the gate signal for T_2 is the logical NOT of the gate signal for T_1, as well as the gate signal for T_4 is the logical NOT of the gate signal for T_3, to avoid short circuit on each leg.

Fig. 4 shows the gate signals V_{g1}, V_{g2}, V_{g3} and V_{g4}.

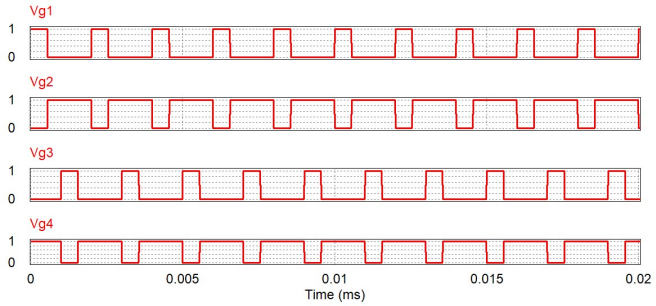

Fig. 4. Gate signals of T_1, T_2, T_3 and T_4

If D and 0° are respectively the duty-cycle and the phase shift of V_{g1}, the other gate signals have therefore duty-cycle and phase shift features as reported in Table IV.

TABLE IV. GATE SIGNALS FEATURES IN FULL-BRIDGE PWM

Gate signal	Duty-cycle	Phase Shift
V_{g1}	D	0°
V_{g2}=NOT of V_{g1}	1-D	0°
V_{g3}	D	180°
V_{g4}=NOT of V_{g4}	1-D	180°

Particular attention should be paid to the power transferred to the primary winding of the transformer. In particular, three different states for the primary winding voltage can be defined: the highest value, which is equal to 100 V, is obtained when T_1 and T_4 are on, and T_2 and T_3 are off; the lowest value, which is equal to -100 V, is obtained when T_2 and T_3 are on, and T_1 and T_4 are off; the third value, which is 0, is obtained when T_1 and T_3 are off, and T_2 and T_4 are on, or vice versa.

The interval time Δt_0, in which this voltage is 0, is function of the duty-cycle: the lower this last one is, the longer this interval time is:

$$\Delta t_0=(0.5\text{-}D)\cdot T_{sw} \quad (12)$$

In this way, the power transferred to the primary circuit of the transformer can be controlled and therefore the load power can be controlled too.

The transformer secondary winding voltage supplies the four-diode rectifier: when it is high, the diodes D_1 and D_4 are on, and D_2 and D_3 are off; when it's 0, all diodes are off; when it's low, D_2 and D_3 are on, and D_1 and D_4 are off.

Finally, the output capacitor is used for providing to the resistive load a stable voltage.

IV. Simulation Results

The analysis of the full-bridge circuit has been carried out by considering its three subsections: the full-bridge inverter (DC-AC), transferring power from the DC supply to the primary winding of the transformer; the transformer (AC-AC); the rectifier (AC-DC), transferring power from the secondary winding to the load.

The power supply, the real powers transferred to each winding and the load power are referenced as P_E, P_{t1}, P_{t2} and P_{out} respectively, so that three different efficiencies can be defined:

$$\eta_{inv}=\frac{P_{t_1}}{P_E} \quad (13)$$

$$\eta_{tr}=\frac{P_{t_2}}{P_{t_1}} \quad (14)$$

$$\eta_{rect}=\frac{P_{out}}{P_{t_2}} \quad (15)$$

The total load-supply efficiency is therefore:

$$\eta_{tot}=\eta_{inv}\cdot\eta_{tr}\cdot\eta_{rect} \quad (16)$$

Efficiencies measures as resulting from the performed simulations have been carried out by maintaining the output power costant and by varying the switching frequency. The duty-cycle has been chosen in order to set the load power to 200 W.

The frequencies range within which efficiencies have been measured goes from 20 kHz to 600 kHz.

For each section, the input power and the output power have been processed; the current and voltage waveforms concerning primary and secondary side of the transformer are shown in Fig. 6.

The circuit efficiencies measured by using silicon devices are shown in Fig. 6.

The inverter efficiency η_{inv} is generally close to 1 in so far as conduction power losses, due to the 9 mΩ MOSFET channel resistance, are very low; with increasing frequency, it decreases because of switching losses.

Instead, by using SiC devices, the efficiency curves shown in Fig. 7 have been obtained.

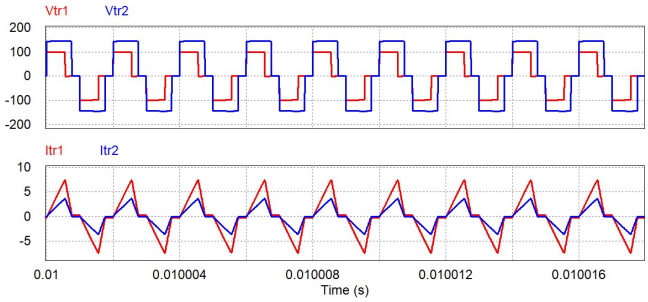

Fig. 5. Primary winding and secondary winding voltage and current signals: the voltage waveforms are highlighted in red colour, whereas the current waveforms are highlighted in blue colour.

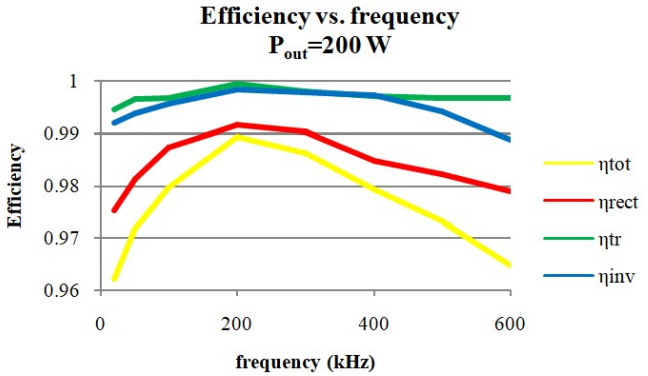

Fig.6. Efficiency curves as resulting from simulation on Si-based converter.

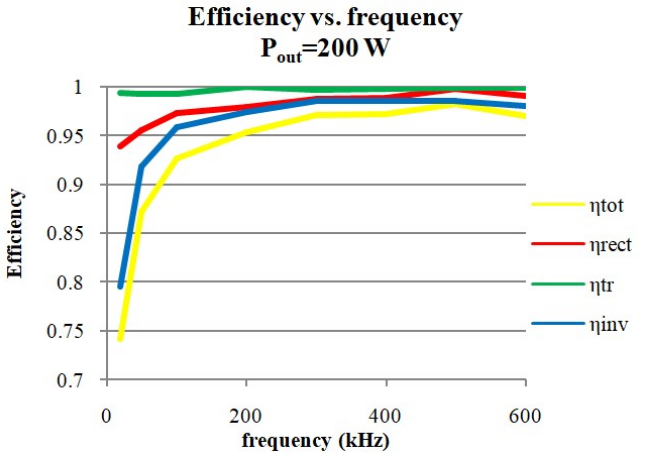

Fig. 7. Efficiency curves as resulting from simulation on SiC-based converter.

As can be seen, because of the 75 mΩ MOSFET channel resistance, conduction power losses are higher than the silicon ones; for this reason, η_{inv} efficiency referred to SiC devices is lower than the inverter efficiency measured by using silicon devices; with reference to the transformer subsection, in both cases, η_{tr} is about unitary while, with increasing frequency, η_{rect} efficiency measures are higher than those ones obtained by using silicon devices: the trend of the graph is about constant, while the silicon η_{rect} graph is degressive in so far as t_{rr} and Q_{rr} in SiC diodes are null; therefore, SiC diodes produce fewer switching power losses with respect to the silicon diodes.

By comparing the total DC-DC efficiency curves to each other, the graph in Fig. 8 is obtained.

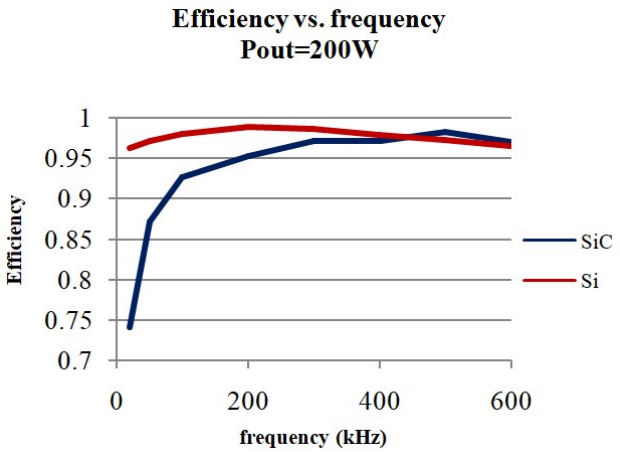

Fig. 8. Comparison between the curves of total efficiency between Si and SiC case.

The graphs demonstrate that, at frequencies ranging from 20 kHz to 400 kHz, switching power losses aren't significantly high and the circuit efficiency measured by using silicon devices is higher than the efficiency obtained by using the SiC devices; therefore, SiC conduction losses are higher than the silicon ones; instead, with increasing frequency, SiC devices produce fewer losses compared to the silicon ones: because of their low internal capacitances and low reverse recovery parameters, SiC MOSFETs and diodes deliver very low switching power losses with respect to the silicon devices; therefore, SiC exploitation at high frequency is recommended.

V. Conclusions

In this paper, an investigation on the different behaviour of Si and SiC power MOSFETs has been carried out in terms power losses for a DC-DC isolated converter with several possible applications, such as in the automotive field. In order to demonstrate the remarkable advantages of the SiC devices over the silicon ones for the highest frequencies, the converter working has been simulated by means of PWM control under different switching frequencies, up to 600 kHz. Although the selected Si MOSFET has a better conduction resistance, the SiC devices offer better performances in terms of efficiency at the highest frequencies, allowing the opportunity of a notable mass and size reduction of the filtering networks as well as of the transformer. Simulation tests have been performed by means of *PowerSIM* software, after an accurate work of components modeling.

Acknowledgment

This work was realized with the contribution of: PON R&I 2015-2020 PROpulsione e Sistemi IBridi per velivoli ad ala fissa e rotante PROSIB, CUP no:B66C18000290005; PRIN 2017, Advanced power-trains and -systems for full electric aircrafts , prot. no.: 2017MS9F49; RPLab (Rapid Prototyping Laboratory - University of Palermo); project REACTION (first and euRopEAn siC eighT Inches pilOt liNe), co-funded by the ECSEL Joint Undertaking under grant agreement No 783158 [33]; PON R&I 2014-2020 - AIM (Attraction and International Mobility), project AIM1851228-1; SDES (Sustainable Development and Energy Savings) Laboratory UNINETLAB of University of Palermo, Laboratory of Electrical APplications LEAP - of University of Palermo.

References

[1] Meng, Zhun & Wang, Yi-Feng & Yang, Liang & Li, Wei. (2017). Analysis of Power Loss and Improved Simulation Method of a High Frequency Dual-Buck Full-Bridge Inverter. Energies. 10. 311. 10.3390/en10030311., p. 1

[2] W. Zhang, L. Zhang, P. Mao and Y. Hou, "Characterization of SiC MOSFET switching performance," *2018 1st Workshop on Wide Bandgap Power Devices and Applications in Asia (WiPDA Asia)*, Xi'an, China, 2018, pp. 100-105, doi: 10.1109/WiPDAAsia.2018.8734560., p. 1

[3] Online - https://www.rohm.com/products/sic-power-devices

[4] V. Boscaino, F. Pellitteri, G. Capponi, R. La Rosa, "A wireless battery charger architecture for consumer electronics", International Conference on Consumer Electronics, ICCE 2012, Berlin, Germany, September 3-5, pp. 84-88; 2012.

[5] Pellitteri, F., Caruso, M., Castiglia, V., Miceli, R., Spataro, C., Viola, F., "Experimental Investigation on Magnetic Field Effects of IPT for Electric Bikes", (2018) Electric Power Components and Systems, 46 (2), pp. 125-134.

[6] V. Cecconi, V. Di Dio, A. O. Di Tommaso, S. Di Tommaso, D. La Cascia and R. Miceli, "Active power maximizing for Wind Electrical Energy Generating Systems moved by a Modular Multiple Blade Fixed Pitch Wind Turbine," *2008 International Symposium on Power Electronics, Electrical Drives, Automation and Motion*, 2008, pp. 1460-1465.

[7] Boscaino, V., Miceli, R., & Capponi, G. (2013). MATLAB-based simulator of a 5 kW fuel cell for power electronics design. *International Journal of Hydrogen Energy*, *38*(19), 7924-7934.

[8] M. Caruso, V. Castiglia, A. O. Di Tommaso, R. Miceli, F. Pellitteri, L. Schirone, "An inductive charger for automotive applications", Industrial Electronic Society Conference, IECON 2016, Florence, Italy, October 24-27, pp. 4482-4486; 2016.

[9] Cipriani, G., Di Dio, V., La Cascia, D., Miceli, R., & Rizzo, R. (2013). A novel approach for parameters determination in four lumped PV parametric model with operative range evaluation.

[10] F. Pellitteri, V. Boscaino, R. Miceli, U. K. Madawala, "Power tracking with maximum efficiency for Wireless Charging of E-bikes", International Electric Vehicle Conference, IEVC 2014, Florence, Italy, December 17-19, pp. 1-7; 2015.

[11] V. Di Dio, R. Miceli, C. Rando and G. Zizzo, "Dynamics photovoltaic generators: Technical aspects and economical valuation," *SPEEDAM 2010*, 2010, pp. 635-640.

[12] F. Pellitteri, V. Boscaino, R. La Rosa, G. Capponi, "Improving the efficiency of a standard compliant wireless battery charger", Universities Power Engineering Conference, UPEC 2012, London, UK, September 4-7, pp. 1-6; 2012.

[13] C. Cecati, F. Genduso, R. Miceli and G. Ricco Galluzzo, "A suitable control technique for fault-tolerant converters in Distributed Generation," *2011 IEEE International Symposium on Industrial Electronics*, 2011, pp. 107-112.

[14] G. Schettino, I. Colak, A. O. Di Tommaso, R. Miceli and F. Viola, "Innovative Computational Approach to Harmonic Mitigation for Seven-level Cascaded H-Bridge Inverters," *2020 Fifteenth International Conference on Ecological Vehicles and Renewable Energies (EVER)*, Monte-Carlo, Monaco, 2020, pp. 1-7.

[15] F. Viola, P. Romano, E. R. Sanseverino, R. Miceli, M. Cardinale and G. Schettino, "An economic study about the installation of PV plants reconfiguration systems in Italy," *2014 International Conference on Renewable Energy Research and Application (ICRERA)*, 2014, pp. 989-994.

[16] F. Pellitteri, V. Boscaino, A. O. Di Tommaso, R. Miceli, "Efficiency optimization in bi-directional inductive power transfer systems", International Conference on Electrical Systems for Aircraft, Railway, Ship Propulsion and Road Vehicles, ESARS 2015, Aachen, Germany, March 3-5, pp. 1-6; 2015.

[17] ST – SCTH40N120G2V7AG datasheet, pp. 1-4
https://www.st.com/resource/en/datasheet/scth40n120g2v7ag.pdf

[18] L. Schirone, F. Pellitteri, "Energy Policies and Sustainable Management of Energy Sources", *Sustainability,* 2017, *9*(12), 2321; doi:10.3390/su9122321, pp. 1-13.

[19] V. Castiglia, N. Campagna, C. Spataro, C. Nevoloso, F. Viola and R. Miceli, "Modelling, simulation and characterization of a

supercapacitor," *2020 IEEE 20th Mediterranean Electrotechnical Conference (MELECON)*, Palermo, Italy, 2020, pp. 46-51.

[20] F. Pellitteri, V. Castiglia, P. Livreri, R. Miceli, "Analysis and design of bi-directional DC-DC converters for ultracapacitors management in EVs", International Conference on Ecological Vehicles and Renewable Energies, EVER 2018, Monte-Carlo, pp. 1-6; 2018.

[21] R. Beibei, W. Dan, M. Chengxiong, Q. Jun and Z. Jiangang, "Analysis of full bridge DC-DC converter in power system," *2011 4th International Conference on Electric Utility Deregulation and Restructuring and Power Technologies (DRPT)*, Weihai, China, 2011, pp. 1242-1245, doi: 10.1109/DRPT.2011.5994085., p. 1

[22] Mohan – Power Electronics, pp. 5, 588, 589

[23] Infineon Technologies – Power Management & Supply, CoolMOS - How to Select the Right CoolMOS TM and its Power Handling Capability, pp. 14, 18, 19
https://www.infineon.com/dgdl/Infineon-ApplicationNote_MOSFET_CoolMOS_How_to_select_the_right_CoolMOS-AN-v01_00-EN.pdf?fileId=db3a304412b407950112b40acf580693

[24] Infineon Technologies - Dr. Dušan Graovac, Marco Pürschel,
Andreas Kiep - MOSFET Power Losses Calculation Using the Data-Sheet Parameters, pp. 3,4
https://application-notes.digchip.com/070/70-41484.pdf

[25] POWERSIM – PSIM User's Manual, p. 160
https://www.powersimtech.com/wp-content/uploads/2021/01/PSIM-User-Manual.pdf

[26] ST - Calculation of conduction losses in a power rectifier – p. 6
https://www.st.com/resource/en/application_note/cd00003894-calculation-of-conduction-losses-in-a-power-rectifier-stmicroelectronics.pdf

[27] Online - https://efficiencywins.nexperia.com/efficient-products/qrr-overlooked-and-underappreciated-in-efficiency-battle.html

[28] ST - Calculation of turn-off power losses generated by an ultrafast diode – pp.3, 4, 9
https://www.st.com/resource/en/application_note/dm00380483-calculation-of-turnoff-power-losses-generated-by-a-ultrafast-diode-stmicroelectronics.pdf

[29] USCi - Turn-Off Characteristics of SiC JBS Diodes, pp. 2,3
https://unitedsic.com/appnotes/USCi_AN0011Turn-Off-Characteristics-of-SiC-JBS-diodes.pdf

[30] IOR International Rectifier – IRFB4410ZPbF, IRFS4410ZPbF IRFSL4410ZPbF datasheet, p. 2
https://eu.mouser.com/datasheet/2/196/irfb4410zpbf-1732505.pdf

[31] Infineon – IDD05SG60C datasheet, pp.1-2
https://www.infineon.com/dgdl/Infineon-IDD05SG60C-DS-v02_04-en.pdf?fileId=db3a304327b897500127dd2fc4391a74

[32] ONSemiconductor – MUR3020WT, MUR3060WT datasheet, pp.2, 5
https://pdf1.alldatasheet.com/datasheet-pdf/view/174422/ONSEMI/MUR3020WT.html

[33] *The first and euRopEAn siC eighT Inches pilOt liNe: A project, called REACTION, that will boost key SiC Technologies upgrading (developments) in Europe, unleashing Applications in the Automotive Power Electronics Sector*, Messina, A.A., Calabretta, M., ...et others, 2020 AEIT International Conference of Electrical and Electronic Technologies for Automotive, AEIT AUTOMOTIVE 2020